

# Activated Fibers: Fiber-centered Activation Detection in Task-based fMRI

Jinglei Lv<sup>1</sup>, Lei Guo<sup>1</sup>, Kaiming Li<sup>1,2</sup>, Xintao Hu<sup>1</sup>, Dajiang Zhu<sup>2</sup>, Junwei Han<sup>1</sup>,  
Tianming Liu<sup>2</sup>

<sup>1</sup> School of Automation, Northwestern Polytechnical University, Xi'an, China,

<sup>2</sup> Department of Computer Science and Bioimaging Research Center,  
The University of Georgia, Athens, GA, USA.

**Abstract.** In task-based fMRI, the generalized linear model (GLM) is widely used to detect activated brain regions. A fundamental assumption in the GLM model for fMRI activation detection is that the brain's response, represented by the blood-oxygenation level dependent (BOLD) signals of volumetric voxels, follows the shape of stimulus paradigm. Based on this same assumption, we use the dynamic functional connectivity (DFC) curves between two ends of a white matter fiber, instead of the BOLD signal, to represent the brain's response, and apply the GLM to detect Activated Fibers (AFs). Our rationale is that brain regions connected by white matter fibers tend to be *more* synchronized during stimulus intervals than during baseline intervals. Therefore, the DFC curves for fibers connecting active brain regions should be positively correlated with the stimulus paradigm, which is verified by our extensive experiments using multimodal task-based fMRI and diffusion tensor imaging (DTI) data. Our results demonstrate that the detected AFs connect not only most of the activated brain regions detected via traditional voxel-based GLM method, but also many other brain regions, suggesting that the voxel-based GLM method may be too conservative in detecting activated brain regions.

**Keywords:** fMRI, DTI, activated fibers

## 1 Introduction

Human brain is an inter-linked network that is wired by neuronal axons. In vivo DTI provides non-invasive mapping of the axonal fibers [1] that connect brain regions into structural networks. It is widely believed that human brain function is a network behavior, e.g., brain network oscillation in the resting state [2, 3] or synchronization of nodes within networks during task performance [4]. Therefore, it is natural and intuitive to incorporate structural network information into the study of human brain function. In our view, it is straightforward to consider a white matter fiber inferred from DTI tractography as the finest possible resolution of structural network that is composed of two gray matter voxels on its ends. Then, the level of functional synchronization of the fiber's two ends, measured by the temporal correlation of raw fMRI signals, can be used as the indicator of the fiber's functional state. For instance, high functional synchronization means engagement in a certain task, while low functional synchronization indicates random behavior [4]. Hence, in this paper, we utilize the temporal functional synchronization of two end voxels of white matter

fibers, measured by DFC, to represent the brain's responses to stimulus paradigm and apply the GLM to detect activated fibers.

The major innovations and contributions of this paper are as follows. 1) Instead of using raw fMRI BOLD signals to detect activated brain regions as used in many popular fMRI data analysis software packages such as FSL, SPM, and AFNI, we propose to use the DFC curves (represented by temporal correlation of fMRI BOLD signals at two ends of a fiber) to detect activated fibers and brain regions. In comparison, the raw fMRI signal measures BOLD activity at the voxels level, while DFC measures the *functional connectivity* of structurally connected brain regions. From a neuroscience perspective, the DFC reflects network-level response to paradigm stimuli, while fMRI raw signal reflects local voxel-level response to the stimuli. From a signal processing perspective, DFC is more robust to noises and has less non-stationarity, while raw fMRI BOLD signals has considerable noise and non-stationarity. 2) The framework is intuitive, effective and efficient. Our experimental results using multimodal working memory task-based fMRI and DTI data are promising. All of the computational components in this framework are based on well-established techniques such as functional connectivity measurement and the GLM method. Therefore, the framework can be easily deployed to many applications, once multimodal DTI and fMRI data is available.

## 2 Method

### 2.1 Overview of the method

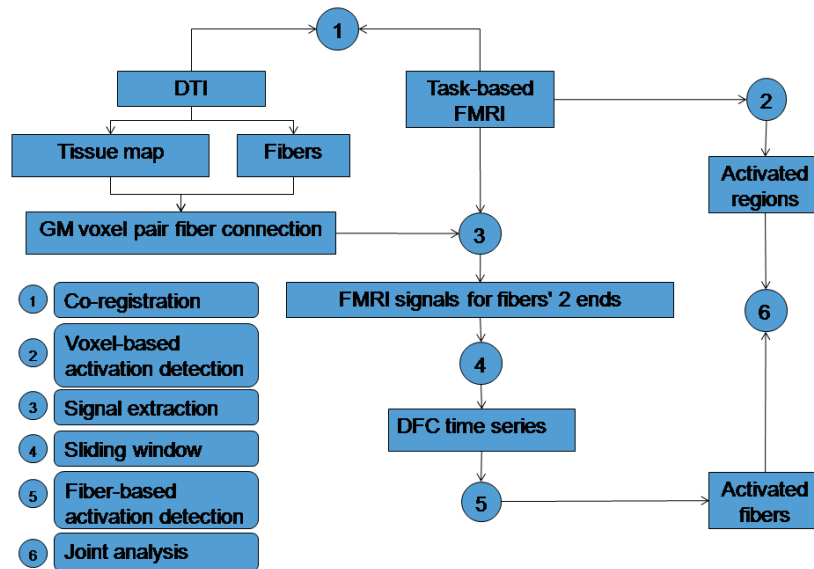


**Fig.1.** The flowchart of the proposed computational pipeline for fiber-centered activation detection in task-based fMRI. The six steps are explained in the left bottom corner.

The proposed computational pipeline is summarized in Figure 1. Firstly, in step 1, we co-registered the task-based fMRI dataset into the DTI space using a linear

registration method integrated in the FSL FLIRT (<http://www.fmrib.ox.ac.uk/fsl/>). For a given fiber tract, the gray matter (GM) voxels connected to its two ends were identified with the guidance of the brain tissue map derived from DTI dataset [7]. With the co-registered fMRI dataset, the fMRI BOLD time series of the identified GM voxels were attached to the fiber, as shown in Step 3. In general, the functional state of the fiber in response to input stimuli is measured by the functional connectivity between its two ends. Thus, in Step 4, a sliding window approach was used to capture the temporal dynamics of the functional connectivity, resulting in a functional connectivity time series and it is referred to as dynamic functional connectivity (DFC) hereafter. Similar to many existing approaches, the functional connectivity is defined as the temporal correlation between the fMRI BOLD signals. The widely used General Linear Model (GLM) [17] was then used to perform activation detection based on the DFC for all the fibers, as shown in Step 5. Finally, joint analysis (Step 6) was conducted between the activated fiber detection result and the conventional voxel-based activation detection result obtained in Step 2.

## 2.2 Data acquisition and preprocessing

In the OSPAN working memory task-based fMRI experiment [6], 23 subjects were scanned and fMRI images were acquired on a 3T GE Signa scanner. Briefly, acquisition parameters were as follows:  $64 \times 64$  matrix, 4mm slice thickness, 220mm FOV, 30 slices, TR=1.5s, TE=25ms, ASSET=2. Each participant performed a modified version of the OSPAN task (3 block types: OSPAN, Arithmetic, and Baseline) while fMRI data was acquired. DTI data were acquired with dimensionality  $128 \times 128 \times 60$ , spatial resolution  $2mm \times 2mm \times 2mm$ ; parameters were TR 15.5s and TE 89.5ms, with 30 DWI gradient directions and 3 B0 volumes acquired.

The fMRI data was co-registered to the DTI space using a linear transformation via FSL FLIRT. For fMRI images, the preprocessing pipelines included motion correction, spatial smoothing, temporal prewhitening, slice time correction, global drift removal [5-8]. For DTI data, preprocessing included skull removal, motion correction and eddy current correction. Brain tissue segmentation was conducted on DTI data using a similar method in [9]. Since DTI and fMRI sequences are both echo planar imaging (EPI) sequences, the misalignment between DTI and fMRI images is much less than that between T1 and fMRI images [7]. The cortical surface was reconstructed from the brain tissue maps using in-house software [10]. The fiber tracking was performed using the MEDINRIA package [11].

## 2.3 Fiber projection

It was reported in the literature that blood supply to white matter is significantly lower than that of the cortex (less than one fourth) [13]. Hence, the fMRI signals in white matter (WM) are less meaningful and our analysis will only focus on the investigation of gray matter (GM) connected by fiber tracts.

Unfortunately, the ends of fiber tracts are not necessarily located on the cortex. The reasons are at least two folds. First, the FA (fractional anisotropy) values around the boundaries of gray matter and white matter are relatively low and the tractography procedure might stop before reaching the cortex. As a result, the tracked fibers will

not be within the cortical surface. Second, there is discrepancy in the brain tissue segmentation based on DTI data and the DTI tractography. In this case, the fiber could be either outside the cortex if the gray matter is over-segmented or inside the cortex if the gray matter is under-segmented, as reported in the literature [12].

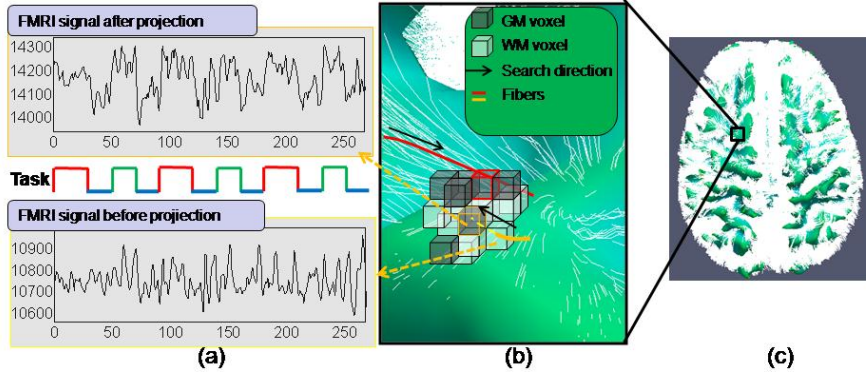


**Fig.2.** Illustration of white matter fiber projection. The joint visualization of white matter fiber tracts (white curves) and the GM/WM cortical surface (green mesh) is shown on the right (c). The zoomed-in view of the black rectangle is shown in the middle (b). The fMRI BOLD signal of one end of a fiber before and after fiber projection is shown on the left (a). The stimulus paradigm curve is also shown in the middle of (a).

To project the fibers onto the GM cortex, we use the brain tissue map (WM, GM and CSF) derived from DTI dataset as guidance for accurate projection, as illustrated in Figure 2. In specific, denotes an end point of a fiber as  $N_e(x_e, y_e, z_e)$  and the point adjacent to  $N_e$  as  $N_{e-1}(x_{e-1}, y_{e-1}, z_{e-1})$ . We define the forward direction as  $\vec{d}_f = N_e - N_{e-1}$  and the backward direction  $\vec{d}_b$  as  $-\vec{d}_f$ . If  $N_e$  corresponds to a non-brain (outside the brain) or CSF voxel in the brain tissue map (e.g., the red fiber tract shown in Figure 2), we search along backward direction  $\vec{d}_b$  until reaching the gray matter. If  $N_e$  corresponds to a WM voxel in the brain tissue map (e.g., the orange fiber tract shown in Figure 2), we search along forward direction  $\vec{d}_f$  until reaching the GM. If  $N_e$  already corresponds to a GM voxel in the brain tissue map, no search is conducted. The search is conducted iteratively until at least one GM voxel can be found in the 1-ring neighborhood of the current seed point, or the number of iteration exceeds a given threshold. When multiple GM voxels exist, the closest one is used as the projected point. In very rare cases when the corresponding GM voxel cannot be found for the end point of a fiber, this fiber is considered as an outlier and discarded. After the fiber projection, two GM voxels were identified for a fiber at its two ends and the corresponding fMRI BOLD signals were attached to that fiber. A comparison for extracted fMRI BOLD signals before and after projection is shown in Figure 2a. It is evident that the extracted fMRI signal from GM voxel after fiber projection has a similar shape as the input stimulus curve, while the fMRI signal extracted before fiber projection does not. This example demonstrates that projection of fibers to GM voxels is critical to extraction of meaningful fMRI BOLD signals.

## 2.4 Dynamic functional connectivity of fiber-connected brain regions

White matter axonal fibers, serving as structural substrates of functional connectivity among brain regions, have abundant functional features [3, 14]. In this paper, we define the dynamic functional connectivity (DFC) between a fiber's two ends to monitor the state of the fiber under stimulus. The functional connectivity is quantified as the temporal Pearson correlation between the two fMRI BOLD signals attached to the fiber. A sliding window approach is adopted to capture the functional connectivity in the temporal domain, as illustrated in Figure 3.

Specifically, given a fMRI dataset with the total length of  $t$  (unit in volume) and the sliding window with the width of  $t_w$ , at each time point  $t_n$ , we extract a signal window with length  $t_w$  centered at  $t_n$  to calculate the functional connectivity. Note that for the first and last few time points in the fMRI BOLD signal, the window length was shortened to calculate DFCs. After sliding over all the time points, the resulted DFCs have the same length as the original fMRI signals. Figure 3 provides illustrations of the DFC calculation procedure. The same DFC calculation procedure is performed for all of the fibers in the whole brain obtained from DTI tractography, and thus we convert voxel-based fMRI signals to fiber-centered DFC signals.

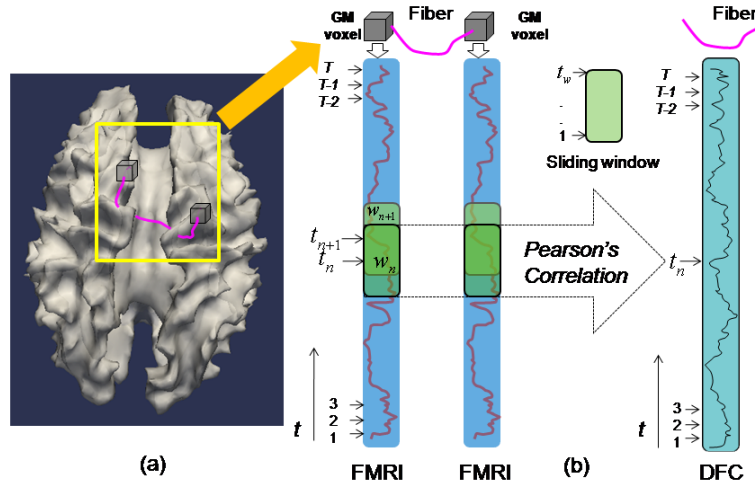


**Fig.3.** Illustration of DFC calculation. (a). Illustration of extracting GM voxels (gray boxes) at the two ends of a fiber, represented by the purple curve. (b) A sliding window approach is applied on two raw fMRI signals and the DFC is calculated.

## 2.5 Activated Fibers Detection

The GLM model [17] has been widely used for task-based fMRI activation detection, which will be adopted here as well. In our fiber-based activation detection, we treat the DFC time series of fibers as inputs to the model for activation detection (Fig. 3), instead of the raw fMRI signals, and use FSL FEAT (<http://www.fmrib.ox.ac.uk/fsl/>) to generate the activation map of fibers for the task-based fMRI data. Fig. 4 provides an illustration of the computational pipeline for fiber-centered activation detection. In

specific, we treated each fiber as a voxel and mapped all of the white matter fibers (around 30,000-50,000 in our dataset) to a virtual volume (Fig. 4). Then, the DFCs of all the fibers are stacked into a 4D volumetric images. By such conversion, FSL FEAT can be directly used for activation detection. After the activation detection, fibers whose corresponding virtual voxels were detected as activated are considered as activated (right bottom figure in Fig. 4).

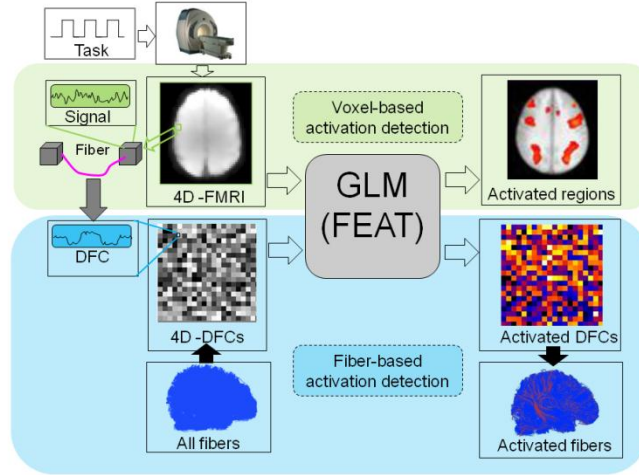


**Fig.4.** Overview of the computational pipeline for fiber-centered activation detection. The voxel-based activation detection is shown in the top panel and the fiber-based activation detection is shown in the bottom panel.

In addition, the z-statistic value for each virtual voxel is mapped to the corresponding fiber as metric of its activation level. Different thresholds can then be used to achieve various activation maps. It should be noted that we performed GLM on the DFC of each fiber independently, as similar in the voxel-based GLM method in FSL FEAT. The statistical correlation procedures for false positive control such as the Gaussian random field theory [15] or false discovery rate method [16] have not been implemented in this paper yet, in that statistical modeling of correlation between fibers is still an open problem and will be left to our future work.

### 3 Experimental Results

In this section, the GLM was applied to detect activated voxels based on the task-based fMRI data and to detect activated fibers based on the framework described in sections 2.3-2.5. The width of the sliding window ( $t_w$ ) used in DFC calculation is set as 15 times of TR in the following experiments.

#### 3.1 Comparison of fMRI signal and DFC

As a comparison study, we first calculated the Pearson correlation coefficients between the fMRI BOLD signals and the stimulus curve (convolved with hemodynamic response function), as well as the Pearson correlation coefficients between DFC curves and the stimulus. The distributions of the two sets of correlation

coefficients over the entire brain are shown in Figure 5 as an example. It is noted that both of the statistics were conducted over the projected fMRI signals of all fiber ends. It is evident in Fig. 5 that the DFC curves have much higher correlations with the stimulus curve, as indicated by the higher accumulations in histogram bin with high correlations.

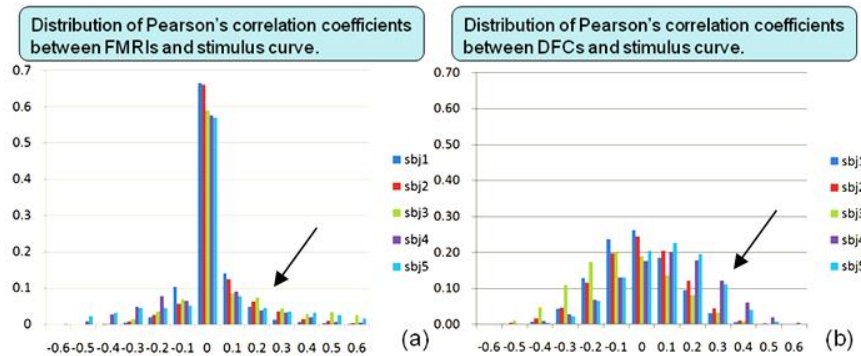


**Fig.5.** Comparison of distributions of Pearson's correlation coefficients. The horizontal axis represents the histogram bins and vertical axis is the Pearson correlation. (a) The distribution of the Pearson correlations between raw fMRI signals and the stimulus curve. (b) The distribution of the Pearson correlations between DFCs and the stimulus curve. Five subjects represented by different colors are shown in the figure.

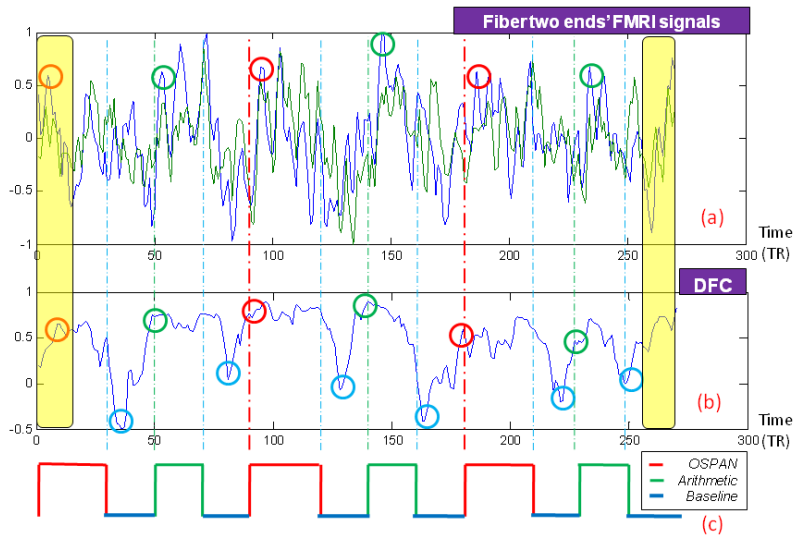


**Fig.6.** Comparison of fMRI signals and DFC curve. (a) BOLD signals of two activated GM voxels that are connected by a fiber (one in blue, the other in green). (b) DFC curve of the fiber connecting the two GM voxels. (c) The time line of the input stimuli (OSPAN, arithmetic and resting). Circles in different colors correspond to different stimuli. Note that, as mentioned in section 2.3, the length of the sliding window for the start and end time points is relatively shorter, so the DFC curves in the yellow regions are not considered.

Figure 6 visualizes one example, in which two GM voxels were activated in the voxel-based activation detection. The fMRI BOLD signals of the two GM voxels are shown in Figure 6a. The DFC of the activated fiber connecting the two GM voxels is shown in Figure 6b. In comparison, the fMRI signals show high level of noises, while the DFC shows much higher signal-to-noise ratio. In addition, the DFC curve shows a high level of stationarity during stimulus intervals (starting with the red and green circles in Figure 6b). Meanwhile, during resting time intervals (baseline), the DFC curve shows a significant valley (blue circles), which is much more stable and robust than the raw fMRI signals in Figure 6a. In short, the DFC curves are much more synchronized with the stimulus curve than the raw fMRI signals. The results in Figure 5 and 6 support our previous premise that DFCs reflect brain's network-level responses to stimulus and provide significantly better contrasts between brain states during stimulus and baseline intervals in task-based fMRI.

### 3.2 Global view of DFCs

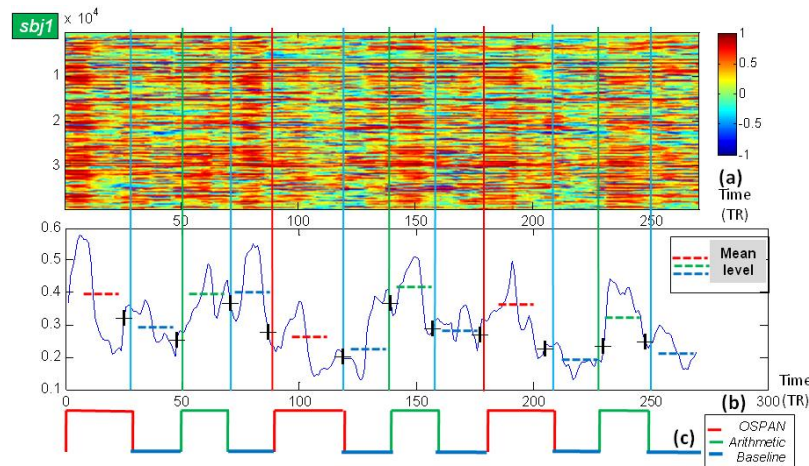


**Fig.7.** Global view of DFCs of all the fiber tracts in the entire brain for one subject. (a) The color coded DFCs of all fibers. Color bar is on the right. Totally, about 38,000 fibers are stacked into each column. The vertical axis represents the index of fibers, and the horizontal axis is the timeline. (b) Average DFC over all fiber tracts. (c) Input stimulus. Three types of blocks are color-coded.

In this subsection, we examine the global pattern of DFCs of all the fibers in the brain. Figure 7 presents a global view of DFCs for one subject (with around 38,000 fibers). The DFC curves are color-coded and stacked into a matrix, as shown in Figure 7a. We can see that significant portion of the fibers have similar temporal patterns in responses to the stimulus curve (Figure 7b). Meanwhile, the averaged DFC over all of the fibers in Figure 7b shows that the brain's overall response is in synchronization with the stimulus curves to some extent. Black pluses in Figure 7b indicate that when the stimulus changes, and the global state of the brain represented by the average DFCs also change sharply in response to the input stimulus curve. These results are reproducible in all of the cases we studied, and Figure 8 shows another example. The above results suggest that white matter fibers are much more synchronized during

stimulus intervals than during baseline intervals, and DFCs are meaningful representations of the brain's responses to stimuli.

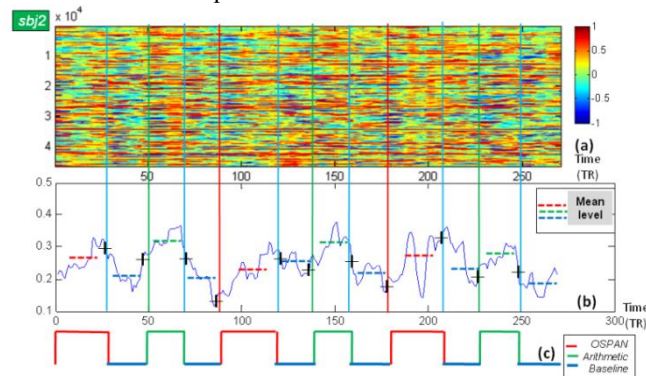


**Fig.8.** Another example of global view of DFCs of all the fiber tracts (around 45,000 fibers) in the entire brain. The settings are similar as those in Fig. 7.

### 3.3 Statistics analysis of activated fibers

In this subsection, we examine the spatial distribution of  $z$ -statistic values of the fibers in the whole brain. As an example, the histograms of the  $z$ -statistic values of all fibers in five brains for two types of stimulus (OSPAN and arithmetic contrasts in the working memory task [6]) are shown in Figure 9. It is evident that the global patterns of the histograms are quite similar across different types of stimuli, and the histogram patterns for different brains are also quite similar. However, the spatial distributions of the  $z$ -statistic values for all the fibers in response to different stimuli are quite different, as shown in Figure 10. For better visualization, the fibers in the entire brain of three subjects are color-coded using the  $z$ -statistic values in Figure 10. The fibers in red have  $z$ -statistic values over 3. As shown in the exemplar regions highlighted by black circles, the  $z$ -statistic value maps corresponding to the two types of stimuli show different patterns (Figure 10a and 10b). This result is quite reasonable considering the brain regions that are activated in these two tasks, as shown in Figure 11 and in [6]. At the same time, activation patterns for the same type of stimuli are reasonably consistent across subjects, as demonstrated by the three subjects in Figure 10. The results in Figure 9 and 10 demonstrate the reliability of fiber-based activation detection in our methods.

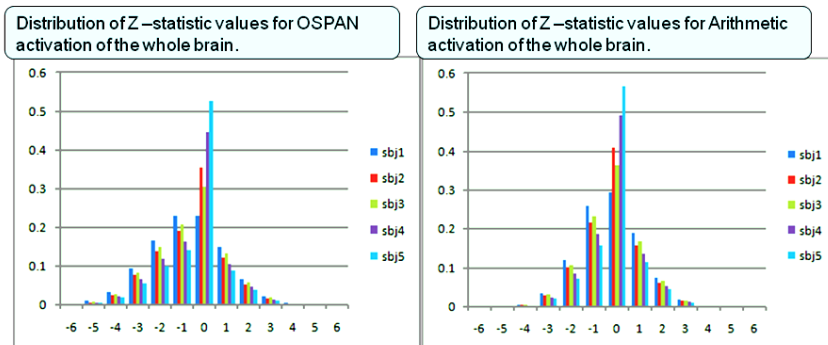


**Fig.9.** Histograms of z-statistic values for two types of stimuli (OSPAN and Arithmetic respectively) for 5 subjects.

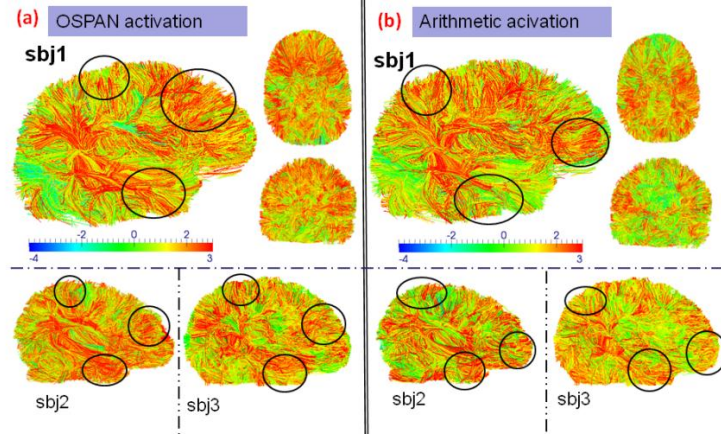


**Fig.10.** Color-coded z-statistic values for fibers under two different stimuli. The color bars are in the middle. (a) Fibers under OSPAN stimulus. (b) Fibers under arithmetic stimulus. Both (a) and (b) show three subjects. Three views from different angles are shown for subject 1. Regions in black circles highlight example regions with consistent patterns across subjects under the same stimulus.

### 3.4 Comparison of fiber-centered and voxel-based activation detections

Based on the activated fibers, we then detect activated brain regions via a straightforward mapping approach, i.e., any cortical or subcortical regions penetrated by the activated fibers are considered as activated brain regions. As an example, Figure 11 demonstrates that the activated fibers were mapped to cortical surface regions they connect to (red regions in Figure 11b and 11e). For comparison, the conventional voxel-based activations were also mapped onto the cortical surface (white regions in 11a and 11d). The voxel-based activated regions in Figure 11a and 11d were also overlaid on the activated regions in Figure 11b and 11e, respectively, as shown in Figure 11c and 11f. It is apparent that the activated regions detected in voxel-based method are a subset of the ones detected with our fiber-centered method, which partly demonstrates the validity of our methods. This result is reproducible in all of the cases we studied, suggesting that our fiber-centered method has better sensitivity in detecting activations than traditional voxel-based method.

Finally, we adopted different z-statistic value thresholds (from 3.5 to 5) to determine the activated fibers and thus activated brain regions in our method, and the results are shown in Figure 12. The activated regions by the voxel-based method are kept the same as those in Figure 11 and in [6]. It is apparent that increasing the z-statistic threshold will result in less activated fibers and brain regions, as shown in Figure 12a – 12d. It is striking that most of the regions obtained by the voxel-based method are consistently included in a subset of the detected brain regions by our method, suggesting the good sensitivity and robustness of our fiber-centered method. The results in Figure 12 further indicate that our fiber-centered method has better sensitivity than traditional voxel-based method. We believe the better sensitivity of our fiber-centered activation detection method is *not* due to false positives, because

our extensive experimental results in Figure 6 – 10 consistently demonstrated that fibers are significantly more synchronized during stimulus intervals than during baseline intervals.

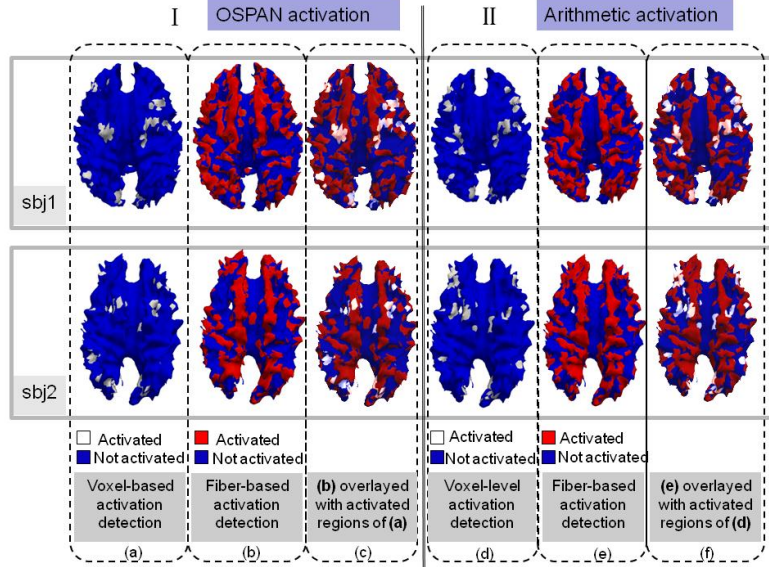


**Fig.11.** Joint visualization of activated regions detected by voxel-based and fiber-centered GLM methods. Z-statistic value of 4 was used as threshold. (a)~(c): Activated regions for OSPAN stimulus resulted from the conventional voxel-based activation detection and our fiber-centered method. (d)~(f): Activated regions for arithmetic stimulus resulted from these two methods.

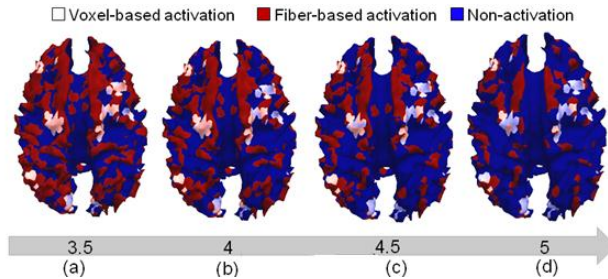


**Fig.12.** Fiber-centered detection results using different z-statistic thresholds. (a)-(d): thresholds from 3.5 to 5, respectively. The activated regions by voxel-based method are overlaid on all of the results by fiber-centered methods.

## 4 Conclusion

We presented a novel framework for detection of activated fibers in task-based fMRI. In comparison with traditional voxel-based GLM activation detection, our framework is able to detect more activated brain regions that are connected by white matter fibers with similar temporal patterns as the input stimulus paradigm. Our experimental results showed that many more fibers are significantly synchronized during task intervals, providing direction support to the concept of activated fibers. Then, the

brain regions at the two ends of activated fibers are considered as participating in the task and thus are considered as activated regions. The experimental results in Figure 11 and 12 show that activated regions detected in traditional voxel-based GLM method are a subset of the activated regions detected by our method, partly supporting the validity of our framework. In the future, we will apply this framework to other multimodal task-based fMRI and DTI dataset, in order to further evaluate and validate this framework. Also, we will develop and evaluate statistical analysis methods to control the false positive detections in the activated fiber detection.

## References

1. Basser PJ, Mattiello J, LeBihan D (1994). Estimation of the effective self-diffusion tensor from the NMR spin-echo. *Journal of Magnetic Resonance Series B* 103 (3): 247–254.
2. Bharat B. Biswal, Toward discovery science of human brain function, *PNAS* March 9, 2010 vol. 107 no. 10 4734–4739.
3. M.D. Fox, and M.E. Raichle, Spontaneous fluctuations in brain activity observed with functional magnetic resonance imaging, *Nat Rev Neurosci*, 8(9): p. 700–11, 2007.
4. Friston, K., Modalities, modes, and models in functional neuroimaging. *Science*, vol.326, no.5951, 399–403(2009).
5. X. Hu, F. Deng, K. Li et al., “Bridging Low-level Features and High-level Semantics via fMRI Brain Imaging for Video Classification,” in *Proceedings of the ACM Multimedia*, 2010.
6. C. C. Faraco, D. Smith, J. Langley et al., “Mapping the Working Memory Network using the OSPAN Task,” *NeuroImage*, vol. 47, no. Supplement 1, pp. S105–S105, 2009.
7. K. Li, L. Guo, G. Li et al., “Cortical surface based identification of brain networks using high spatial resolution resting state FMRI data,” in *Proceedings of the 2010 IEEE international conference on Biomedical imaging: from nano to Macro*, Rotterdam, Netherlands, 2010, pp. 656–659.
8. J. Lv, L. Guo, X. Hu et al., "Fiber-Centered Analysis of Brain Connectivities Using DTI and Resting State FMRI Data," *Medical Image Computing and Computer-Assisted Intervention – MICCAI 2010, Lecture Notes in Computer Science* T. Jiang, N. Navab, J. Pluim et al., eds., pp. 143–150: Springer Berlin / Heidelberg, 2010.
9. T. Liu, H. Li, K. Wong et al., “Brain tissue segmentation based on DTI data,” *NeuroImage*, vol. 38, no. 1, pp. 114–123, 2007.
10. T Liu, et al., “Deformable Registration of Cortical Structures via Hybrid Volumetric and Surface Warping”, *NeuroImage*,22(4):1790–801, 2004.
11. <http://www-sop.inria.fr/asclepios/software/MedINRIA/>.
12. D. Zhang, et al., Automatic cortical surface parcellation based on fiber density information. *IEEE International Symposium on Biomedical Imaging (ISBI)*, Rotterdam, 2010, 1133–1136.
13. Aviv Mezer, et al., Cluster analysis of resting-state fMRI time series. *NeuroImage*, 45 (2009) 1117–1125.
14. C.J. Honey, et al., "Predicting human resting-state functional connectivity from structural connectivity," *PNAS*, 106(6): p. 2035–40, 2009.
15. K. J. Worsley, et al., A unified statistical approach for determining significant voxels in images of cerebral activation. *Human Brain Mapping*, 4:58–73, 1996.
16. Christopher R. Genovese, Nicole A. Lazar, Thomas E. Nichols, Thresholding of Statistical Maps in Functional Neuroimaging Using the False Discovery Rate. (2002). *NeuroImage* 15:870–878.

17. K.J. Friston, et al.: Statistical Parametric Maps in Functional Imaging: A General Linear Approach. *Human Brain Mapping*. 1995, 2:189-210.